

A Geometric Method to Constrain Emission Regions of Pulsars

Hong-Guang Wang¹, Guo-Jun Qiao², Ren-Xin Xu² and Yi Liu¹

¹ Center for Astrophysics, Guangzhou University, Guangzhou 510006, China

² Department of Astronomy, Peking University, Beijing 100871, China

Abstract A geometric method that attempts to synthesize all available geometric information on a pulsar is developed to constrain the 3-D structure of emission regions of pulsars. In terms of retarded magnetic dipolar field and with inclusion of aberration and retardation effects, the method is endeavored to constrain the geometrical parameters of emission regions via reproducing observational multi-wavelength features, e.g. pulse widths, phase offsets between different pulses and polarization properties. It is applied to gamma-ray pulsar B1055–52 which shows main pulse and inter-pulse at radio frequencies and double-peaked light curve at gamma-ray energy band. The results imply that the radio emission region probably consists of an inner and an outer ring, while the gamma-ray emission region is severely asymmetrical to magnetic axis.

Key words: pulsars: individual: PSR B1055–52 — radiation mechanisms: non-thermal

1 INTRODUCTION

Although extensive progresses have been made on both observation and theories on pulsars since the first discovery of pulsar in 1967, we do not have comprehensive answers for many basic problems, one of which is where the multi-band emission originate in pulsar magnetosphere. On the one hand, it is commonly agreed that radio emission heights are about a few percent of the radius of light cylinder (see Wu et al. 2002 and references therein). However, the structure of radio emission region remains controversial. Some authors suggested that the emission beam consists of a few (normally two) homocentric cones and a central core (e.g. Rankin 1983; Gil & Krawczyk 1996). To generate these components one needs either a few conal and a core emission zones coaxial to magnetic axis (e.g. the sparking model, Ruderman & Sutherland 1975; Gil & Sendyk 2000) or one emission zone but different emission heights to produce different beams (e.g. the ICS model, Qiao 1988; Qiao & Lin 1998). Some other authors argued that the radio emission beam is not cone/core-like but patchy (Manchester 1995; Han & Manchester 2001). In this case the structure of emission region may be somewhat arbitrary. On the other hand, there is also no consensus about the gamma-ray emission region. In the literatures the polar cap model (Harding 1981; Daugherty & Harding 1996), the outer gap model (Cheng, Ho, & Ruderman 1986a, b; Cheng, Ruderman, & Zhang 2000), the two-pole caustic model (Dyks & Rudak 2003), the slot gap model (Muslimov & Harding 2004), and the annular gap model (Qiao et al. 2004) have been proposed to account for the γ -ray emission of pulsars, in which the suggested emission locations are different from each other. Therefore, it is very necessary to make independent constraints on the emission regions to test those models. In this paper we present a synthetically geometric method to constrain multi-wavelength emission regions from observational properties and the preliminary results of its application to gamma-ray pulsar B1055–52.

2 THE GEOMETRIC METHOD

The main idea of the method is as follows. In pulsar magnetosphere photons are emitted from a group of open field lines, thus forming multi-wavelength emission beams. The observed pulse widths are related to

* E-mail: wanghg@gzhu.edu.cn

beam size (or spatial extent of the emission regions) as well as the inclination angle α and the viewing angle ζ between the line of sight (hereafter LOS) and the rotation axis. The phase offsets between various pulses are attributed to the original phase offsets due to separation of field lines and additional offsets caused by aberration and retardation effects. Beside pulse widths and phase offsets, some other emission properties, e.g. polarization are related to structure of emission regions as well. Therefore, the emission regions can be constrained by fitting these observational features.

This method includes three basic assumptions. (1) The magnetic field lines of a rotating pulsar follow a retarded dipolar field (Cheng et al. 2000). It has a benefit that the rotational sweep back effect can be inherently included. Although the retarded dipolar field is only an approximate solution for vacuum magnetosphere, for lack of better solutions, it is assumed to approximately represent the real magnetic field of a plasma-loaded magnetosphere. (2) In the co-rotation reference frame, the emission direction (hereafter initial emission direction) is assumed to be along the tangent of magnetic field line. The $1/\gamma$ solid angle of emission cone of a relativistic particle is neglected for the purpose of simplified calculation. (3) The emission patterns are assumed to be the same at two opposite poles. Thus, if different parts of emission region are constrained for the opposite poles, we can combine the results and reconstruct the whole emission region at one pole.

In order to describe the 3-D structure of emission region we need to know on which open field lines the emission is generated and the emission heights therein. So the outputs of the method are three geometrical parameters, viz. the emission height r counted from the stellar centre to an emission point, the azimuthal angle φ of the star-surface-footprint of a field line from which emission is generated and a factor η defined as $\eta = \theta_\varphi/\theta_{\varphi,0}$, where φ and θ are defined in the spherical coordinate system of which the polar axis is magnetic axis, φ is counted anticlockwise when observing towards the stellar centre from each pole, θ_φ is the polar angle of the foot point of an open field line on polar cap surface, the subscript “0” denotes the last open field line. Parameter η varies from 0 (the magnetic axis) to 1 (the last open field lines). A smaller value of η means that the field line is more inner or closer to the magnetic axis.

In practice the method operates in two steps. An outline for each step is shown below, details and formulae will be presented elsewhere (Wang et al.). As an example, the following procedure is applicable to a pulsar with high-quality data of radio polarization and radio/gamma-ray pulse profiles.

Step 1, determining geometrical parameters of the pulsar and finding out all possible emission regions that can viewed by our line of sight. (1) Determine or constrain the values of α and ζ . Sometimes they can be obtained by fitting the observed position angles of linear polarization with rotation vector model (hereafter RVM, Radhakrishnan & Cooke 1969). Definite values of α and ζ will greatly reduce the numerical calculation. (2) Numerically trace the open magnetic field lines (a function of α and coordinates) and calculate the modified emission direction at various points for each open field line by involving aberration effect. (3) Select all the emission points where the emission direction is aligned with our LOS. The criterion used here is that the angle between the modified emission direction and rotational axis equals to ζ . In sub-step (2), since there is no simple analytic equations to describe the rotating magnetic dipole, we develop a numerical code to trace magnetic field lines. To calculate the modified emission direction we first figure out the initial emission direction in the co-rotation reference frame and then obtain the direction in laboratory reference frame via Lorentz transform.

Step 2, constraining the emission regions via fitting the observed polarization and pulse profile properties. In this step the emission points that can reproduce the observed properties are picked out from all the possible emission points. (1) First the longitudes of the emissions from all possible emission points are figured out. (2) Then these longitudes are tested to reproduce the observed properties. Only the emission points that can reproduce all the properties are selected. For a typical gamma-ray pulsar the observed properties include (a) The radio and gamma-ray pulse widths, (b) the phase separation between radio main pulse and inter-pulse (if it has), (c) the phase offset between radio and gamma-ray pulses and (d) radio polarization properties, viz. linear polarization percentage and phase offset between the position angle sweep and pulse profile. In the first sub-step one need consider not only aberration but also retardation effect, because retardation effect affects the relative longitudes of emissions which come from different heights.

3 APPLICATION TO PSR B1055–52

PSR B1055–52 is a unique object among seven known gamma-ray pulsars. It shows radio main pulse and inter-pulse and double-peaked gamma-ray light curve at above 240 MeV (see figure 1, Thompson et al. 1999). The main observation properties used by the method are as follows. (a) The pulse widths of radio main pulse, inter-pulse and gamma-ray pulse are 32° (at 10%-level of peak intensity), 44° (at 20%-level of peak intensity to avoid noise) and 90° (peak-to-peak separation), respectively. (b) The phase offset between the main pulse and inter-pulse is 157° . (c) The trailing gamma-ray peak precedes the centre of radio main pulse by about 12° . (d) The sweeps of the position angle (hereafter PA) of linear polarization follow “S” shapes across both main pulse and inter-pulse, the maximum slope rates of PA are approximately 1.6 and 7.0, respectively. (e) The main pulse is nearly fully linear polarized. But the case is quite different in inter-pulse. The linear polarization percentage is nearly 100% at the leading edge of inter-pulse, then it decreases to about 80% at the leading peak and rapidly drops down below $\sim 10\%$ at the trailing component. (f) For radio main pulse no significant offset appears between the centre of PA curve (where the maximum PA slope rate is reached) and the centre of pulse profile. In inter-pulse the PA sweep shows to be half of a full “S” shape that predicted by standard RVM. The above radio and gamma-ray data are measured from Lyne & Manchester (1988, hereafter LM88) and Thompson et al. (1999).

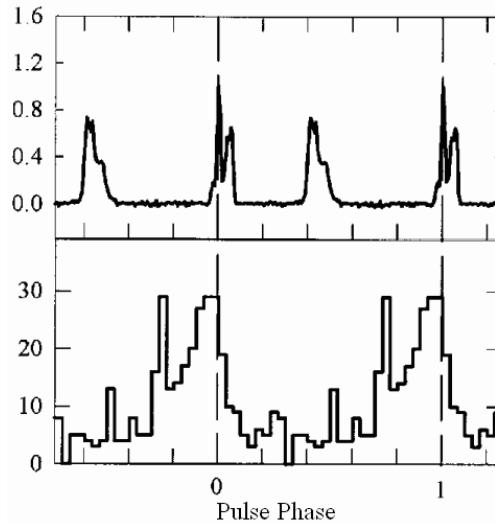


Fig. 1 The radio profile at 1.5 GHz and gamma-ray light curve of B1055–52 at above 240 MeV (Thompson et al. 1999). The radio phase reference is shown by a vertical dashed line.

The PA data can be fitted very well by standard RVM at both 640 MHz (LM88) and 950 MHz (van Ommen et al. 1997). The best fit values of (α, ζ) at both frequencies are consistent to each other, which are $(74.7^\circ, 113.4^\circ)$ and $(78^\circ, 112^\circ)$, respectively.

Some authors suggested that the radio main pulse and inter-pulse come from opposite poles (LM88, Biggs 1990; van Ommen et al. 1997). Our detailed analysis on the PA sweep and main-inter-pulse phase separation supports this scenario (Wang et al. 2005). The polar origin of the gamma-ray pulse can be self-consistently determined in the constraining procedure. It is found that the gamma-ray pulse should be emitted from the same pole as the radio main pulse, otherwise the observed gamma-ray pulse width and the phase offset between radio and gamma-ray pulses can not be coherently explained.

With the known inclination and viewing angles and polar origin of pulse components, we use the method to constrain r , η and φ . The results are presented in Table 1 for the emission regions from which the radio main pulse, the leading and trailing parts of inter-pulse and gamma-ray pulse originate, respectively. Note that the results represent the emission points that can be seen by LOS. In column 3 negative/positive

Table 1 Constraint on the parameters of radio and gamma-ray emission regions. MP, IP and GP indicate main pulse, inter-pulse and gamma-ray pulse, respectively.

Emission region	η ($^{\circ}$)	φ ($^{\circ}$)	r/r_c	r/r_{NCS}
	$\alpha = 78^{\circ}$,	$\zeta = 112^{\circ}$		
MP	0.90 ~ 1.00	-35 ~ 20	0.11 ~ 0.18	7.45 ~ 7.84
IP Leading	0.80 ~ 1.00	61 ~ 67	0.13 ~ 0.26	--
IP trailing	0.32 ~ 0.60	0 ~ 54	0.06 ~ 0.30	--
GP Leading	0.90 ~ 1.00	46 ~ 55	0.45 ~ 0.69	10.1 ~ 13.4
GP trailing	0.90 ~ 1.00	14 ~ 49	0.13 ~ 0.47	7.70 ~ 9.91
	$\alpha = 74.7^{\circ}$,	$\zeta = 113.4^{\circ}$		
MP	0.90 ~ 1.00	-33 ~ 18	0.13 ~ 0.21	5.42 ~ 5.78
IP Leading	--	--	--	--
IP trailing	0.20 ~ 1.00	0 ~ 66	0.06 ~ 0.28	--
GP Leading	0.90 ~ 1.00	45 ~ 54	0.45 ~ 0.65	7.06 ~ 8.63
GP trailing	0.90 ~ 1.00	11 ~ 47	0.15 ~ 0.49	5.70 ~ 7.43

value of azimuthal angle φ represents the field line on the trailing/leading side of meridian. Leading and trailing sides are defined with respect to the direction of stellar rotation. In general emission from leading side appears in the leading phase of pulse profile. In columns 4 and 5 the emission height r is presented in unit of the radius of light cylinder r_c and the local radius of null charge surface r_{nCS} at the same field line, respectively. The values of (α, ζ) derived by LM88 and van Ommen et al. are both used. No solution is obtained for emission of the leading component of inter-pulse with $\alpha = 74.7^{\circ}$ and $\zeta = 113.4^{\circ}$, so it shows that the group $(74.7^{\circ}, 113.4^{\circ})$ is not so successful as the other group in obtaining full solutions.

From the above results the 3-D structure of emission regions that are viewed by LOS is summarized as follows:

- (1) The radio main pulse region locates on the lower side of open volume (nearer to the equatorial plane) and concentrates within a very thin layer near the last open lines. The layer extends a bit asymmetrically on both sides of the meridian with a total range of azimuthal angle $\sim 55^{\circ}$. The altitudes extend from $\sim 10\%$ to $\sim 20\%$ of r_c , but they are about 6 times higher than those of the null charge surface.
- (2) The radio inter-pulse region locates on the upper side of open volume nearer to rotation axis. It is very likely composed of two bunches of open field lines. The outer one, being very close to the last open field lines, locates on the leading side of the meridian and is far away from it. The inner one lies in the midway between magnetic axis and last open field lines, and is more extended. The emission altitudes extend to as much as 30% of r_c .
- (3) The gamma-ray emission region locates on the lower side of open volume and also on the leading side of the meridian. It is likely to be within a thin layer near the last open field lines, although the possibility that it is extended towards the magnetic axis can not be excluded yet. The emission altitudes extend from 10% to 70% of r_c .
- (4) The gamma-ray and inter-pulse emission regions are strongly asymmetrical to the meridian, in fact, the results show that our LOS nearly misses all the gamma-ray and inter-pulse emissions from the trailing side (if the pulsar does have these emissions). The asymmetry should be related to asymmetrical properties of the magnetic field, the structure of emission regions or physical process in different parts of emission regions.

Although we can not see the full emission region directly, the above features of the emission regions that viewed by LOS provide implication for entire radio and gamma-ray emission regions.

Radio emission region probably consists of two rings (the shape is referred to the foots of open field lines on polar cap surface). The outer ring lies near the last open field lines, e.g. $0.9 < \eta < 1.0$. The emission altitude may be within about $0.02r_c$ to $0.2r_c$ or equivalently $180 \text{ km} < r_{\text{min}} < 2000 \text{ km}$. The inner ring, probably wider (e.g. $0.3 < \eta < 0.6$) than the outer one, locates in the midway between last open field lines and magnetic axis. The emission altitude may extend from about $0.05r_c$ to $0.3r_c$.

The whole gamma-ray emission region can not be inferred so definitely, because only the emission from one pole is observed. However, the basic features should include that (1) the emission region extends well beyond the null charge surface, and (2) asymmetry should exist not only between the lower and upper sides of open volume but also between the leading and trailing sides of the meridian.

4 CONCLUSIONS AND DISCUSSION

A geometric method that attempts to synthesize all available geometric information on a pulsar is developed to constrain the 3-D structure of emission regions of pulsars. It has been applied to gamma-ray pulsar B1055–52 which shows main pulse and inter-pulse at radio frequencies and double-peaked gamma-ray light curve. The constrained results imply that the radio emission region probably consists of inner and outer rings and the gamma-ray emission region is severely asymmetrical to magnetic axis.

Besides the gamma-ray pulsars, this method can also be used constrain the radio emission region of radio pulsars with high-quality data of polarization and pulse profiles.

Previous geometrical methods used to make some special assumptions to calculate radio emission heights, e.g. pure dipolar magnetic field, a bunch of field lines where emission comes from (mostly the last open field lines) and symmetry of emission region with respect to meridian (e.g. Gil et al. 1984; LM88, Rankin 1993). With these assumptions and the observed pulse widths, the emission heights can be figured out via a set of geometrical relations. Compared with them, our method has the following advantages. (1) The retarded dipolar field we adopted should be more realistic than a pure dipole. (2) We have no beforehand assumptions on emission regions, therefore our method has better capability to reflect the real structure of emission regions, especially asymmetrical properties. (3) Our method is more synthetical in not only the ways to calculate the emission regions but also the capability in accounting for observation features. Besides the pulse widths, our method is endeavored to explain other multi-wavelength properties, e.g. polarization and pulse phase offsets coherently.

The method will be developed in at least the following aspects. (1) Quantitatively modelling the polarization data. Reproducing the observed linear polarization percentage (or depolarization) and the relative phase shift between PA sweep and pulse profiles usually make strong limitation on the emission regions, because superposition of emissions from a certain extent of emission region can cause depolarization and relative phase shift. At present the boundaries of r , η and φ are constrained by rough estimation to let them satisfy the observed properties of PA sweep. We are to quantitatively model these features by considering superposition of emissions from different layers to give better constraints on the boundaries. Meanwhile, the possible deviation from standard RVM due to this and other effects (e.g. the aberration and magnetic field rotational sweep back effects) needs to be considered too. (2) Considering the effect of $1/\gamma$ solid angle of emission cone. In this case the initial emission direction is no longer only the tangent of magnetic field line but within a cone with typical angular radius of $1/\gamma$. For open field lines near magnetic axis, the curvature radius is usually much larger than those of outer field lines. So larger extent of emission region is expected to be seen at inner field lines. We are to relax the second assumption to find how the $1/\gamma$ effect influences the results.

Acknowledgements We are grateful to Prof. R. N. Manchester, Mr. K. J. Lee, Dr. J. H. Fan and Mr. H. Zhang for their valuable comments and discussions. This work is supported by National Nature Science Foundation of China (10403001, 10373002 and 10573002) and by the allotment of research foundation to 10403001 by Guangzhou University.

References

- Biggs J. D., 1990, MNRAS, 246, 341
- Cheng K. S., Ruderman M.A., Zhang L., 2000, ApJ, 537, 964
- Cheng K. S., Ho C., Ruderman M.A., 1986a, ApJ, 300, 500
- Cheng K.S., Ho C., Ruderman M.A., 1986b, ApJ, 300, 522
- Daugherty J.K., Harding A.K., 1996, ApJ, 458, 278
- Dyks J., Rudak B., 2003, ApJ, 598, 1201
- Gil J., Gronkowski P., Rudnicki W., 1984, A&A, 132, 312
- Gil J., Krawczyk A., 1996, MNRAS, 280, 143

- Gil J.A., Sendyk M., 2000, *ApJ*, 541, 351
Han J.L., Manchester R.N., 2001, *MNRAS*, 320, L35
Harding A.K., 1981, *ApJ*, 245, 267
Lyne A.G., Manchester R.N., 1988, *MNRAS*, 234, 477
Manchester R.N., 1995, *JA&A*, 16, 107
Muslimov A.G., Harding A.K., 2004, *ApJ*, 606, 1143
Qiao G.J., 1988, *Vistas in Astronomy*, 31, 393
Qiao G.J., Lee K.J., Wang H.G. et al., 2004, *ApJ*, 606, L49
Qiao G.J., Lin W.P., 1998, *A&A*, 333, 172
Radhakrishnan V., Cooke D.J., 1969, *Astrophys. Lett.*, 3, 225
Rankin J.M., 1983, *ApJ*, 274, 333
Rankin J.M., 1993, *ApJS*, 85, 145
Ruderman M.A., Sutherland P.G., 1975, *ApJ*, 196, 51
Thompson D.J., Bailes M., Bertsch D.L. et al., 1999, *ApJ*, 516, 297
van Ommen T.D., Alessandro F.D., Hamilton P.A. et al., 1997, *MNRAS*, 287, 307
Wang H. G., Qiao G. J., Xu R. X., Liu Y., 2005, submitted
Wu X. J., Huang Z. K., Xu X. B., 2002, *Chin. J. Astron. Astrophys. (ChJAA)*, 2, 454